Ultra-broadband Bragg concave diffraction grating designs on 220-nm SOI for wavelength demultiplexing

KE LI, 1 JINGPING ZHU, 1,* QIHANG DUAN, 2,3 YUZHOU SUN, 1 AND XIIN HOU1,2

Abstract: The appropriate broadband design of a de/multiplexer can significantly increase the channel number and consequently the transmission capacity of a wavelength division multiplexing system. Herein, we present the first ultra-broadband Bragg concave diffraction grating (CDG) on a 220-nm silicon-on-insulator, covering most of the E, S, C, L, and U telecommunication wavebands spanning from 1.425 to 1.675 μm. A wide-band-gap Bragg mirror is employed to facilitate broadband reflection, with a low diffraction order of grating for a sufficient free spectral range. Numerical simulations show that the proposed approaching blazed concave diffraction grating (AB-CDG) for the two-material case exhibits a high integration, simple fabrication process, and promising spectral performance. We fabricate the grating for design verification with a low transmission loss of -0.6 dB and a crosstalk below -33.7 dB for the eight measured wavelength channels covering the spectral range from 1.5 to 1.61 µm that is limited by the bandwidth of the grating coupler. This design can be used for broadband wavelength demultiplexing, frontier astronomical observation, and spectroscopic imaging.

© 2021 Optical Society of America under the terms of the OSA Open Access Publishing Agreement

Introduction

As the link capacity has increased dramatically, advanced multiplexing technologies have attracted considerable attention in the past decades [1-3]. Wavelength division multiplexing (WDM) has been widely employed in telecommunication schemes to enable the transmission of multiple channels in parallel [4]. The transmission capacity increases linearly with the number of wavelength channels; therefore, the deployment of a much larger wavelength band is attractive for WDM networks that would benefit from a large number of channels [5]. Several broadband laser sources [6–7], modulators [8], nanowaveguides [9] and transmission fibers [10] have been demonstrated in classical optical communication. For a de/multiplexer, one of the crucial devices in a WDM network, it is important to achieve a broadband response with low excess loss. Among the many technologies available, concave diffraction grating (CDG) [11–15], a typical planar integrated circuit, is promising because of its significant advantages of compactness, relaxed fabrication tolerances, and reduced costs. For a conventional CDG, the chromatic dispersion is attained via the wavelength-dependent high-order diffraction from a series of facets of the grating, which leads to a restricted bandwidth scalability [11,16].

A few methods have been reported to extend the operational wavelength range [5,17–20]. Idrisa et al. designed a cyclic arrayed-waveguide grating (AWG) connected with an array of $2 \times$ 1 y-branch couplers on silica-on-silicon with a refractive index difference of $\sim 1\%$, supporting a broad bandwidth of ~250 nm in the T and O bands [5]. However, the device shows a large chip

#431133 Journal © 2021

 $^{^{}I}$ Key Laboratory for Physical Electronics and Devices of the Ministry of Education and Shaanxi Key Lab of Information Photonic Technique, School of Electronic Science and Engineering, Xi'an Jiaotong University, Xi'an 710049, China

 $^{^2}$ Xi'an Institute of Optics and Precision Mechanics, Chinese Academy of Sciences, Xi'an 710119, China ³Xi'an Sino Huaxin Measurement & Control Co., Ltd., Xi'an 710304, China

^{*}jpzhu@xjtu.edu.cn

size of $30 \times 65 \text{ mm}^2$ and a measured insertion loss from -6.4 dB to -8.4 dB. For diffraction grating, Ryckeboer et al. combined four planar concave grating designs on a single chip, each covering a distinct band of tens of nanometers between 1.51 and 2.3 µm [20]. In such a structure, the expansion of the wavelength range is achieved at the cost of a significant increase in the device size. Furthermore, Yang et al. demonstrated an arrayed-input echelle diffraction grating for wavelengths ranging from 1.25 to 1.7 μm, with a 2rd diffraction order and a 160-nm-thick Al layer coated on the facet rear [19]. However, the introduction of a metal coating leads to a high fabrication complexity and strong absorption of light, particularly in the infrared band. The Bragg mirror can realize a high reflectivity approaching 100% without requiring any complex metal coating process [14,21], and it is used for the ultra-broadband CDG design in the present study. Silicon photonics has attracted extensive attention as a promising platform for ultra-compact photonic integrated circuits, owing to its high index contrast, thereby providing a small number of periods of the Bragg mirror [1,11,15]. Furthermore, the attractive compatibility with mature CMOS processes offers mass fabrication at a low cost. Brouckaert et al. have demonstrated a four-channel silicon-on-insulator echelle grating using a second-order Bragg reflector to replace each single facet [22]. However, the discontinuous distribution of Bragg mirrors may introduce an extra transmission loss that occurs at the junction of the two adjacent facets. Furthermore, high-order diffraction limits the further expansion of the diffraction wavelength range.

In this study, we present modeling, design, and fabrication of Bragg-mirror-based ultra-broadband (\sim 250 nm) CDG centered at a wavelength of \sim 1.55 μ m on the standard 220-nm silicon-on-insulator (SOI). A wide-band-gap Bragg mirror is employed to ensure efficient reflection over a wide spectral range, together with a low diffraction order grating providing sufficient free spectral range (FSR). A systematic study of the diffraction bandwidth is presented. To the best of our knowledge, this is the first proposal of ultra-broadband Bragg CDG for a high-index-contrast 220-nm SOI platform, which enables a very small device footprint and a relatively simple fabrication process. The device configuration and design concepts are detailed in Section 2. Broadband derivation under different dimensional and optical parameters and optimization on a silicon photonic platform are presented in Sections 3 and 4, respectively. Section 5 presents the results of the overall device simulations and analysis of the performance of the three optimized configurations. Section 6 demonstrates the fabrication and measurement of the device for the design verification. The proposed design can be utilized in broadband on-chip WDM, and can also be applied in integrated single-photon spectrometers, allowing the probing of a wide variety of molecules.

2. Device configuration and principle

A schematic of the facet position is shown in Fig. 1. The grating is used in a reflective geometry, and instead of a metallized coating, multilayer Bragg mirrors are adopted herein to efficiently reflect the incident light. The grating facets are configured using the 2-stigma method, which enables compact geometries with reduced aberrations [16,23–24], following these rules:

- (1) The extremities of the input and all output waveguides are located on the Rowland circle (RC) with a radius of $R_{\rm rc}$. Q_0 on the circle is set to indicate the central facet center of the grating.
- (2) As shown in Fig. 1(a), there are N_{out} output channels, with the output array center O. O_1 and O_2 are two other output channel centers that are equally spaced on the two sides of O. According to the constructive interference conditions, the path from the input port center I to each facet center Q_j , to the output channel center, should differ from its neighbor facet by an integer number of wavelengths in the slab waveguide, which can be expressed as $l_{1,j+1} l_{1,j} = m\lambda_1/n$ and $l_{2,j+1} l_{2,j} = m\lambda_2/n$. λ_1 and λ_2 are the diffraction wavelengths of O_1 and O_2 , respectively, where n is the effective index of the free propagation region

(FPR). Therefore, the facet center, Q_j , should lie at the intersection of the two ellipses, whose foci are I, O_1 and I, O_2 , respectively. The paths corresponding to the central facet, $l_{1,0}$ and $l_{2,0}$, are calculated first, and thereafter, S facet centers are obtained sequentially on the upper and lower sides of the central facet, respectively, based on the path relationships.

- (3) To avoid additional scattering losses due to intersections or gaps between adjacent teeth, the Bragg reflectors are continuously circular and arranged in a concentric layout with the common center C [21], as shown in Fig. 1(b). Each facet contains N_B periods, and the tilt of these facets provides a blazing effect and establishes a periodicity (period a) along the grating front. The blazing angle of the grating, θ , is associated with the slope of CQ₀.
- (4) Each facet is terminated along $CQ_{j+1/2}$. $Q_{j+1/2}$ is an endpoint between Q_j and Q_{j+1} . The light through $Q_{j+1/2}$ and that reflected from the facet center cancel each other; this is essentially destructive interference. Accordingly, $l_{1,j+1/2} l_{1,j} = m\lambda_1/(2n)$ and $l_{2,j+1/2} l_{2,j} = m\lambda_2/(2n)$ here. Similarly, the position of $Q_{j+1/2}$ is given by the corresponding facet ellipses.

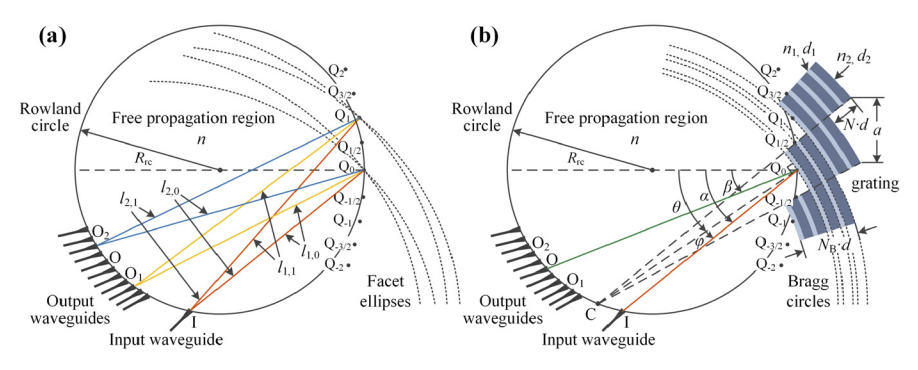


Fig. 1. (a) Schematic of the definition of each facet center of the proposed CDG based on the 2-stigma method. (b) Bragg reflectors arranged in a concentric layout with terminations perpendicular to the facet surface.

The diverging light emanating from the input waveguide with incident angle α relative to the grating normal is diffracted by grating and thereafter refocused to the corresponding output waveguides at angle β . The position of the maximum diffraction intensity depends on the multibeam interference, and the maximum value of the intensity is determined by the single-slit diffraction. From Fig. 1(b), the Bragg period $d=d_1+d_2$, where d_i is the width of the alternating strips with the effective index n_i (i=1 represents the dielectric layer, and i=2 represents the etched layer here). N is the number of Bragg periods per grating period. φ is the incident angle with respect to the normal of the Bragg reflector in the slab region. λ_c is the central wavelength, with the central normalized frequency ϖ_c defined as $\varpi_c = d/\lambda_c$, the diffraction condition is equivalent to [14]

$$m = 2Nn\varpi_{\rm c}\cos\varphi. \tag{1}$$

The multilayer Bragg reflector can be considered as a one-dimensional photonic crystal. The propagation characteristics of the light waves through one period of the Bragg facet are related to a unitary 2×2 translation matrix [25]:

$$\begin{bmatrix} E(x) \\ H(x) \end{bmatrix} = \begin{bmatrix} T_{11} T_{12} \\ T_{21} T_{22} \end{bmatrix} \begin{bmatrix} E(x+d) \\ H(x+d) \end{bmatrix}, \tag{2}$$

$$T_{11} = \cos \delta_1 \cos \delta_2 - \frac{\eta_2}{\eta_1} \sin \delta_1 \sin \delta_2,$$

$$T_{12} = -\frac{i}{\eta_2} \cos \delta_1 \sin \delta_2 - \frac{i}{\eta_1} \sin \delta_1 \cos \delta_2,$$

$$T_{21} = -i\eta_1 \sin \delta_1 \cos \delta_2 - i\eta_2 \cos \delta_1 \sin \delta_2,$$

$$T_{22} = \cos \delta_1 \cos \delta_2 - \frac{\eta_1}{\eta_2} \sin \delta_1 \sin \delta_2,$$

$$(3)$$

where

$$\delta_{i} = k_{i,x}d_{i} = \frac{2\pi n_{i}d_{i}\cos\varphi_{i}}{\lambda_{c}} = \begin{cases} 2\pi n_{1}\varpi_{c}f\cos\varphi_{1}, & i = 1, \\ 2\pi n_{2}\varpi_{c}(1-f)\cos\varphi_{2}, & i = 2, \end{cases}$$

$$(4)$$

and

$$\eta_i = \begin{cases}
\sqrt{\frac{\varepsilon_0}{\mu_0}} n_i \cos \varphi_i, \text{ TE mode,} \\
\sqrt{\frac{\varepsilon_0}{\mu_0}} \cdot \frac{n_i}{\cos \varphi_i}, \text{ TM mode.}
\end{cases}$$
(5)

Here, $k_{1,x}$, $k_{2,x}$, and φ_1 , φ_2 are the wave numbers parallel to the periodic direction and the incident angles relative to the Bragg reflector normal in n_1 and n_2 , respectively. The fill factor is defined as $f = d_1/d$. According to the periodic boundary conditions of the one-dimensional electromagnetic field in the lossless dielectric materials, that is, the Bloch theorem, Eq. (2) can be further written as

$$\begin{bmatrix} E(x) \\ H(x) \end{bmatrix} = \begin{bmatrix} T_{11} & T_{12} \\ T_{21} & T_{22} \end{bmatrix} \begin{bmatrix} E(x+d) \\ H(x+d) \end{bmatrix} = e^{-iKd} \begin{bmatrix} E(x+d) \\ H(x+d) \end{bmatrix}.$$
 (6)

K is the Bloch wave number, which ranges in the first Brillouin zone $\left[-\frac{\pi}{d}, \frac{\pi}{d}\right]$. Furthermore, from Eq. (3), $T_{11} \cdot T_{22} - T_{12} \cdot T_{21} = 1$; *T* is a unimodular matrix. Accordingly, the eigenvalues of *T* are expressed as

$$e^{-iKd} = \frac{1}{2}(T_{11} + T_{22}) \pm \sqrt{\left[\frac{1}{2}(T_{11} + T_{22})\right]^2 - 1}.$$
 (7)

Therefore.

$$\cos(Kd) = \frac{1}{2}(T_{11} + T_{22}) = \cos(\delta_1)\cos(\delta_2) - \rho\sin(\delta_1)\sin(\delta_2), \tag{8}$$

where

$$\rho = \frac{1}{2} (\frac{\eta_1}{\eta_2} + \frac{\eta_2}{\eta_1}). \tag{9}$$

The band edge frequencies, determined by $Kd = M\pi$ with M, the forbidden band order or Bragg order, can be further derived as

$$\cos(\pi \varpi_{\pm} \bar{n}) = \pm \sqrt{\frac{\rho - 1}{\rho + 1} \cos^2(\pi \varpi_{\pm} \nu)}, \quad M \text{ is odd,}$$
 (10)

$$\sin(\pi \varpi_{\pm} \bar{n}) = \pm \sqrt{\frac{\rho - 1}{\rho + 1} \sin^2(\pi \varpi_{\pm} \nu)}, \quad M \text{ is even,}$$
 (11)

where

$$\bar{n} = n_1 f \cos \varphi_1 + n_2 (1 - f) \cos \varphi_2, \tag{12}$$

$$v = n_1 f \cos \varphi_1 - n_2 (1 - f) \cos \varphi_2. \tag{13}$$

The positive and negative signs correspond to the upper and lower boundaries of the forbidden band, respectively. From the Snell-Descartes law,

$$n\sin\varphi = n_1\sin\varphi_1 = n_2\sin\varphi_2. \tag{14}$$

If $\nu \ll \bar{n}$ which is normally true, ϖ_c can be obtained from Eqs. (10) and (11),

$$\varpi_{\rm c} \approx \frac{M}{2\bar{n}}.$$
(15)

Using Eqs. (1), (12) and (15), f can be obtained as

$$f = \frac{\frac{MN}{m}n\cos\varphi - n_2\cos\varphi_2}{n_1\cos\varphi_1 - n_2\cos\varphi_2}.$$
 (16)

The choice of the ratio range of *M* and *m* is obtained from $0 \le f \le 1$, as follows:

$$\frac{n_2\cos\varphi_2}{n\cos\varphi} \le \frac{MN}{m} \le \frac{n_1\cos\varphi_1}{n\cos\varphi}.$$
 (17)

Once the grating configuration $(n, n_1, n_2, \lambda_c, \varphi, \theta, N, m, M)$ has been chosen, ϖ_c can be obtained by Eq. (1), d by $d = \varpi_c \lambda_c$, and f by Eq. (16).

3. Broadband design

For a Bragg-mirror-based CDG, there are two key requirements that must be fulfilled simultaneously to achieve a large bandwidth. One is to guarantee a sufficient FSR,

$$FSR = \frac{\lambda n}{(m+1)n_g - n}.$$
 (18)

 n_g is the group index of the slab. The other key requirement is that the reflector exhibits high reflection over a broad bandwidth. Therefore, a wide-band-gap Bragg mirror is considered here. From Eqs. (9)–(15), the upper and lower band edge frequencies are obtained as [26]:

$$\varpi_{\pm} = \begin{cases}
\varpi_{c} \pm \frac{1}{\pi \bar{n}} \sin^{-1} \left[\sqrt{\frac{\rho - 1}{\rho + 1}} \cos(\pi \varpi_{c} \nu) \right], & M \text{ is odd,} \\
\varpi_{c} \pm \frac{1}{\pi \bar{n}} \sin^{-1} \left[\sqrt{\frac{\rho - 1}{\rho + 1}} \sin(\pi \varpi_{c} \nu) \right], & M \text{ is even.}
\end{cases}$$
(19)

Therefore, the band gap is closely related to refractive indices of the alternating strips. When there is a low index contrast $(n_1 \approx n_2)$, the band gaps would shrink to zero for arbitrary ϖ_c and ν , posing significant challenges to the efficient diffraction for broad wavebands.

Moreover, ν is solved from Eqs. (13) and (16) as

$$v = \frac{Nn\cos\varphi}{m} \cdot g,\tag{20}$$

where

$$g = \frac{M(n_1 \cos \varphi_1 + n_2 \cos \varphi_2) - 2mn_1n_2 \cos \varphi_1 \cos \varphi_2/(Nn \cos \varphi)}{n_1 \cos \varphi_1 - n_2 \cos \varphi_2}.$$
 (21)

Thereafter, the following is obtained:

$$\pi \varpi_{c} \nu = \frac{\pi}{2} \cdot g. \tag{22}$$

When g is an integer and holds opposite parity with the Bragg order M, all the band gaps shrink to zero. On the contrary, all the consistent-parity-order band gaps have a maximum bandwidth,

$$\Delta \lambda_{\text{max}} = \left| \frac{4\pi M \lambda \sin^{-1} \left[\sqrt{\frac{\rho - 1}{\rho + 1}} \right]}{\pi^2 M^2 - 4 \left\{ \sin^{-1} \left[\sqrt{\frac{\rho - 1}{\rho + 1}} \right] \right\}^2} \right|. \tag{23}$$

4. Device optimization on silicon photonic platform

As a proof-of-concept, a Bragg mirror is implemented by exploiting the standard SOI with a 220-nm silicon core thickness, surrounded by silicon dioxide, with an index $n_2 = 1.444$ at the central wavelength, $\lambda_c = 1.55 \, \mu m$. The TE polarization mode is selected here, that is, the electric field is parallel to the slab. A series of stripes are etched down to the silicon layer and replaced by silica. The effective index of the silicon core is considered as $n_1 = 2.848$. The index contrast currently stands at $n_1/n_2 \approx 2$. Furthermore, because the illuminated area of the facets is limited by the incident direction, φ is generally controlled within a reasonable range [27], and is assumed to be zero herein to simplify the analysis. Considering the WDM application and multimode suppression in the 220-nm SOI waveguide, a wide operating spectral range from 1.425 to 1.675 μ m is chosen.

A few particular cases can be considered here based on the above analysis.

For the general three-material case (n is not equal to n_1 or n_2), perfect blazed concave diffraction grating (PB-CDG) can be achieved at the central wavelength λ_c with an appropriate selection of parameters. The extremum of the bandwidth curve is located at the point where g is an integer. In particular, when

$$n = \frac{2mn_1n_2}{MN(n_1 + n_2)},\tag{24}$$

g = 0 is obtained, which indicates the maximum bandwidth for the case with an odd M and the minimum bandwidth for an even M.

The two-material case is then considered. For $n = n_1$, the following equations are obtained from Eqs. (16) and (21):

$$f = \frac{\frac{MN}{m}n_1 - n_2}{n_1 - n_2},\tag{25}$$

$$g = \frac{Mn_1 + \left(M - \frac{2m}{N}\right)n_2}{n_1 - n_2}. (26)$$

If $MN/m \neq 1$, with $n_1/n_2 \approx 2$, then f and g are simplified as

$$f = \frac{2MN}{m} - 1,\tag{27}$$

$$g = 3M - \frac{2m}{N}. (28)$$

If, in addition, N = 1, then g presents the same parity as M. Therefore, the band gap is extremely narrow. If $N \neq 1$, the blazing condition and Bragg condition can be perfectly matched with the appropriate M, M, M, and M selected.

In contrast, if MN/m = 1, then

$$f = 1, g = M. \tag{29}$$

In this case, one of the alternating strips should be infinitely thin. Moreover, the parity of g and M is the same; that is, the Bragg reflector has an extremely narrow band. Therefore, fine

tuning of the fill factor has to be implemented for a sufficient diffraction bandwidth. The blazing condition is not strictly met here. For simplicity, we refer to this grating as the "approaching blazed concave diffraction grating" (AB-CDG).

It should be noted that the low-order diffraction could provide sufficient FSR, and meanwhile prevent a significant reduction in the diffraction efficiency by suppressing unwanted diffraction orders. According to Eq. (1), m is proportional to N. Therefore, N=1 is chosen here for a low diffraction order. As for the Bragg order and diffraction order, there are three main considerations. First, according to Eq. (23), a maximum reflection bandwidth (inversely proportional to M) above 250 nm is allowed for a Bragg mirror on 220-nm SOI with M < 3 (see Fig. 2(a)), contributing to the implementation of broadband diffraction. Thereafter, the diffraction order of m < 6 is limited by the FSR equation. Moreover, from Eq. (17), $\frac{n_2}{n} \le \frac{M}{m} \le \frac{n_1}{n}$ must be satisfied for the stable transmission of guided waves. Consequently, M=m=1 and M=m=2 are selected for the subsequent design.

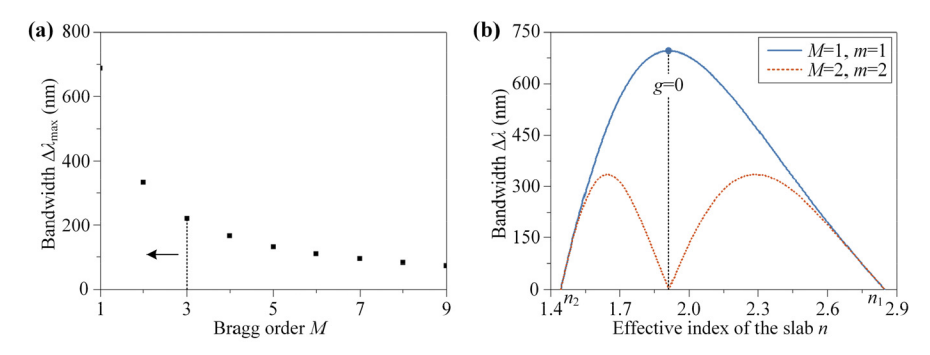


Fig. 2. (a) Maximum reflection bandwidth $\Delta \lambda_{\rm max}$ for different Bragg order M values for the three-material case. (b) Reflection bandwidth $\Delta \lambda$ varying with the effective index of the slab n. The black dashed line marks the chosen design parameters (M=m=1, n=1.916) for the subsequent simulation of the three-material case.

For PB-CDG, n=1.916 is calculated from Eq. (24), indicating the maximum bandwidth for the case of M=m=1 (black dashed line in Fig. 2(b)). On the other hand, for AB-CDG, Fig. 3 shows the variation of the corresponding bandwidth $\Delta\lambda$ and Bragg period d with the fill factor f for the cases M=m=1 and M=m=2. According to Eq. (29), the fill factor should be fine-tuned around 1 to provide sufficient reflection bandwidth with the blazing condition approximately satisfied simultaneously. For the design in this study, f=0.76 represents a viable

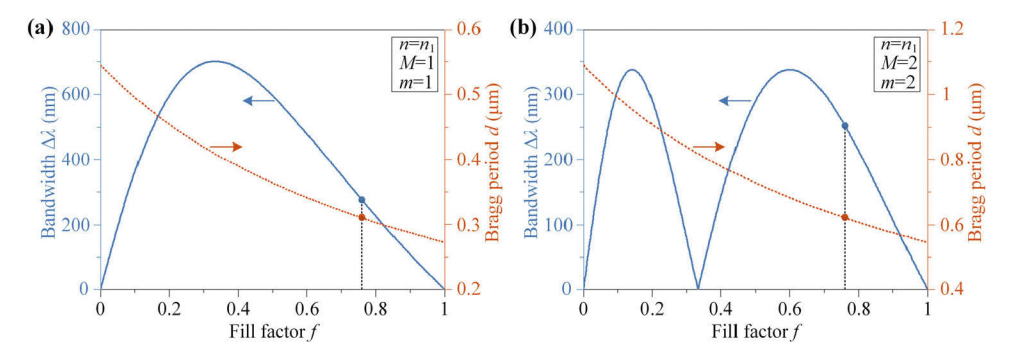


Fig. 3. Bandwidth $\Delta \lambda$ and Bragg period d with different fill factors in the two-material case $(n = n_1)$ for (a)M = m = 1 and (b)M = m = 2. The black dashed line marks the chosen design parameters (f = 0.76) for the subsequent simulation of the two-material case.

compromise between the diffraction bandwidth and efficiency, providing a broad waveband over 250 nm (black dashed line in Fig. 3(a) and Fig. 3(b) for m = 1 and m = 2, respectively).

5. Numerical simulation and discussion

We consider the optimized parameters, described in the previous sections: for the PB-CDG, n=1.916 for the case m=1, as shown in Fig. 2(b); for the AB-CDG, f=0.76, with the corresponding Bragg period, as obtained from Fig. 3. According to the transfer matrix method [28–29], the number of periods of each Bragg facet is chosen to be $N_B=14$. The input waveguides are placed at an incident angle $\varphi=5^\circ$. λ_1 and λ_2 are set as 1.5 and 1.6 µm, respectively. The wavelength spacing of adjacent channels is designed to be 10 nm, allowing for a relatively simple simulation. The output waveguides are aligned along the RC with a center-to-center spacing of approximately 5 µm. The waveguide dimensional parameters, such as the fill factor, Bragg period, and radius of RC, of the three configurations with the same line dispersion capability are listed in Table 1.

PB-CDG Grating parameters 1 2 Effective index n (@1.55 µm) 2.848 2.848 1.916 2 Diffraction order m 1 1 2 Bragg order M 1 Fill factor f0.34 0.76 0.76 Bragg period d (μm) 0.40 0.31 0.62 Blazed angle θ (°) 30 40 40 Incident angle α (°) 35 45 45 Radius of RC R_{rc} (µm) 384 344 344

Table 1. Design parameters of PB- and AB-CDGs.

For the evaluation of the overall device, the numerical simulation of diffraction spectra is conducted using the FDTD Solutions software in a two-dimensional manner, with the multilayer Bragg mirrors and access waveguides included. A 30- μ m-long linear taper is added to facilitate adiabatic propagation and connect the silicon nanowire and the access waveguide from 0.5 μ m to 4 μ m. As expected, all the cases exhibit a high theoretical diffraction efficiency in the designed wideband. A summary of the device performance in terms of the peak transmission loss, non-uniformity, and crosstalk is presented in Fig. 4. Under the same diffraction order, the AB-CDG performs better than the PB-CDG in terms of transmission loss and channel-to-channel variation because of the avoided scattering loss induced by refractive index mutations between the slab region and Bragg reflector. However, the crosstalk between neighboring waveguides shows, on average, an improvement by a few decibels in the PB-CDG compared with that in the AB-CDG, both in terms of the standard deviation and the worst value, which is mainly attributed to the worse aberration in the latter. The mean square error (MSE) of the optical path of each facet center is used to characterize the output deviation of the entire grating to a certain output waveguide. For output point O₁, the MSE at λ_1 is expressed as

$$MSE = \frac{1}{2S+1} \sum_{j=-S}^{S} \left[(l_{1,j} - l_{1,0})n - jm\lambda_1 \right]^2.$$
 (30)

Figure 5 demonstrates the MSEs of the three configurations, which are equivalent at the two aberration-free wavelengths, that is, 1.5 and 1.6 µm. However, at the other wavelengths, AB-CDG

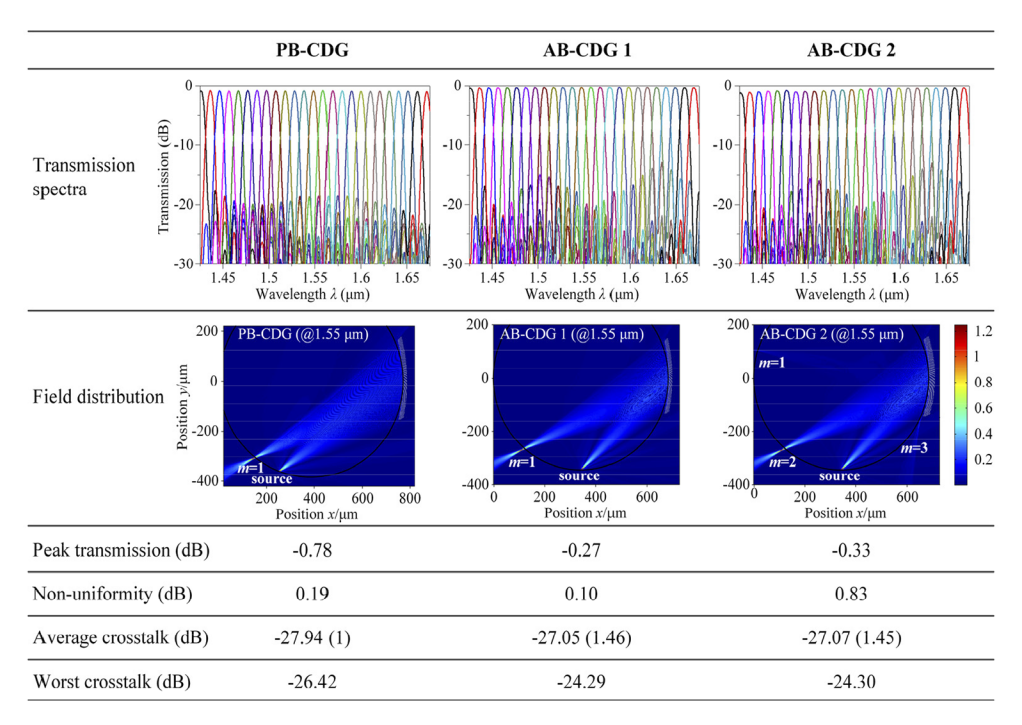


Fig. 4. Simulated results of transmission spectra, field distribution (@1.55 μ m), peak transmission loss, non-uniformity, and crosstalk for the three designed PB- and AB-CDGs.

is inferior to PB-CDG because of its higher index contrast in the slab. This would cause larger output focal spots on the RC of the AB-CDG, resulting in a slightly worse crosstalk between adjacent channels.

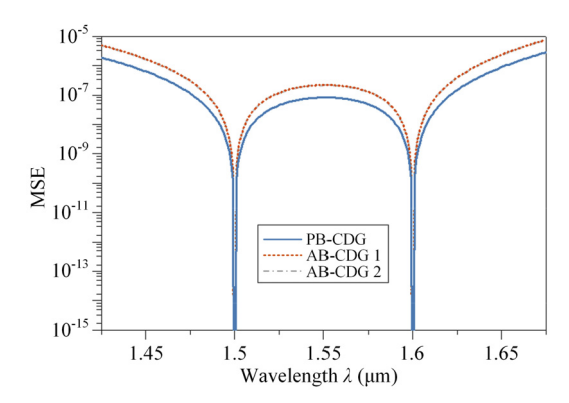


Fig. 5. Mean square error of optical path for the three designed PB- and AB-CDGs.

The AB-CDG, designed for the two-material case, relies exclusively on the standard SOI photonics fabrication processes without using any additional material and is mainly considered here. AB-CDG 1 and 2 show similar waveguide dimensions and MSE values, thereby representing a comparable device integration scale and adjacent crosstalk level. AB-CDG 1 (1st order diffraction case) outperforms AB-CDG 2 in terms of the transmission loss, owing to the inhibition of unwanted multistage diffraction, as can be seen in the field distributions in Fig. 4. However, the

minimum feature size of 74.4 nm in AB-CDG 1 is exactly half of that in AB-CDG 2, which renders the device more sensitive to fabrication uncertainties, leading to higher process requirements.

In general, the three optimized devices exhibit a comparable performance at equidistant wavelengths. The PB-CDG outperforms AB-CDG in terms of the optical path deviation, resulting in a better crosstalk level. However, the AB-CDG, which enables a more compact device size and a relatively simple fabrication process, is more attractive for mass production and is chosen here to ensure a high diffraction efficiency for broad telecommunication wavebands.

Fabrication and measurement

We fabricated the AB-CDG (M=m=2) on a standard SOI material platform with a 220-nm silicon layer and 2-µm buried oxide (BOX) layer. The device was patterned via 193-nm DUV lithography etched by inductively coupled plasma processes down to the BOX layer. Thereafter, a 2-µm top silica layer was deposited via plasma-enhanced chemical vapor deposition. The channel spacing was designed to be 16 nm, with an access waveguide width of 4 µm and $R_{\rm rc}=181$ µm. The minimum radius of the bends was 40 µm, which was also simulated with negligible losses across the desired wavelength range. The width of the silicon nanowire was 0.5 µm, to maintain the single-mode propagation. Grating couplers (GCs) provide off-chip coupling to fibers without the requirement for complicated cutting, grinding, and polishing, as well as precise fine calibration compared with the butt coupler. Optical microscopy images of the fabricated chip are shown in Fig. 6.

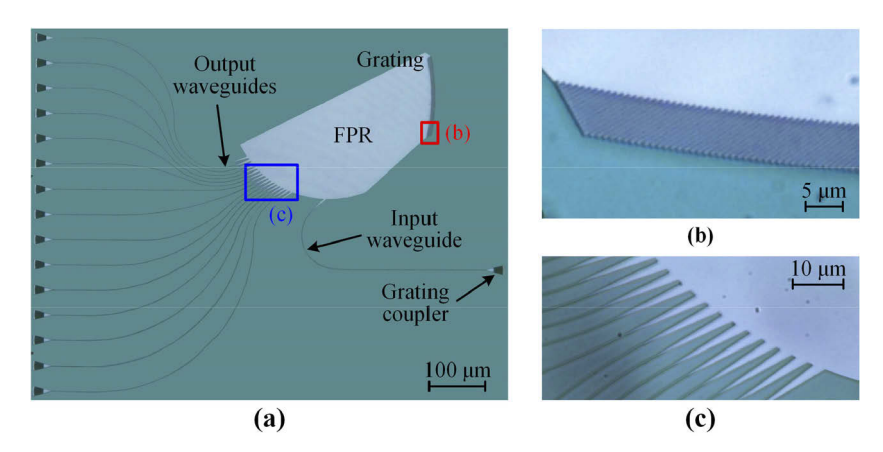


Fig. 6. Optical microscopy images of the fabricated CDG on SOI with grating couplers providing off-chip coupling between the chip and fiber.

To characterize the diffraction grating we use a set-up as shown in Fig. 7. The source of light is a tunable laser (T100S-HP-CL) with a TE-polarized output and spectral range tuned from 1.5 to 1.63 μ m. A polarization controller (PC) is placed in the path of the source for precise control of the output polarized light. To facilitate the coupling and alignment between the optical fiber and chip, an optical branching device (OBD) is used to divide the light from the CDG into two parts, one of which, with 10 percent of the input power, is collected directly by the power meter (PM). An all-band passive optical component tester (Yenista Optics CT400) with an addressable wavelength range from 1.24 to 1.68 μ m is used to offer high-resolution scanning of the other part (90 percent of the input power) at a wavelength step of 0.1 nm. Additional losses induced by the PC and OBD can be compensated by the CT400. The measured spectral range and number of channels in the fabricated device is limited by the bandwidth of the GC (3 dB bandwidth ~40 nm around 1.55 μ m) and detection sensitivity of the CT400 (~-70 dB). The GC encounters significant degradation of performance due to light, with a large deviation from

the central wavelength, which eventually leads to inaccurate measurements of device crosstalk. Therefore, the transmission curves of the device are characterized across the wavelength range from 1.5 to $1.61 \, \mu m$ for the design verification.



Fig. 7. Diagram of measurement system. TL: Tunable Laser; PC: Polarization Controller; CT: Component Tester; DUT: Device Under Test; OBD: Optical Branching Device; PM: Power Meter.

The measured spectra are normalized to a reference straight waveguide with the same waveguide parameters and GC as those used for the CDG. Therefore, except for the coupling loss with input and output fibers, all possible on-chip losses, including Bragg reflection loss, grating diffraction loss, waveguide or slab propagation loss, and coupling loss between the access waveguides and slab region are measured, as shown in Fig. 8. The spectra show a maximum efficiency of -0.6 dB (87%) with channel non-uniformity of approximately 1.9 dB for the eight measured channels. The degraded channel uniformity may be ascribed to the band-shift caused by wafer thickness and refractive index variations, and performance differences among GCs, which can be further improved with precise design of the band gap of Bragg mirror. A relatively low adjacent crosstalk of less than -33.7 dB is realized with a compact footprint of approximately $0.8 \times 0.7 \text{ mm}^2$. The channel spacing is approximately 15.4 nm, which closely matches the expected value and could be decreased by further increasing R_{rc} and by decreasing the separation distance between access waveguides. The slightly deformed spectral shape is mainly caused by the reflection of the GC in the measurement. In comparison, other single CDGs in the 220-nm SOI, have an efficiency ranging from -6.9 dB to -1.9 dB and a crosstalk ranging from -25 dB to -4.3 dB with a bandwidth <90 nm around 1.55 μ m, as reported in previous studies [20,22,30–32]. The demonstrated AB-CDG shows a satisfactory performance at a high efficiency level over a wide spectral range with greater scalability.

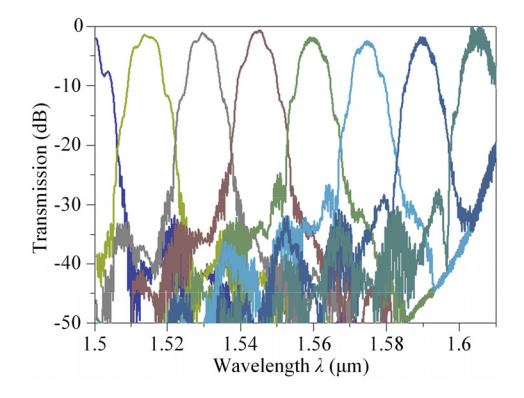


Fig. 8. Experimental transmission spectra of the measured range from 1.5 to 1.61 μm of the fabricated broadband AB-CDG.

7. Conclusion

We have designed and demonstrated the first ultra-broadband concave grating, spanning from 1.425 to 1.675 μm on a 220-nm SOI platform, operating in the TE polarization mode. The design employs a low diffraction order grating to support a wide FSR and simultaneously adopts a multilayer Bragg mirror with a wide photonic band gap to provide efficient and broadband reflection. Computational analysis illustrates that the proposed on-chip AB-CDG supports a broad theoretical diffraction bandwidth of over 250 nm with an improved scalability, and meanwhile exhibits a small device footprint and relatively easy fabrication process. An efficient grating was demonstrated experimentally for the design verification with a state-of-the-art insertion loss of -0.6 dB and a crosstalk lower than -33.7 dB for the measured range of 1.5–1.61 μm at a 16-nm interval. Further differentiated optimization of the GC corresponding to each channel would increase the detection spectral range. The designs presented in this study enables an ultra-broadband, compact and efficient diffraction grating for applications from demultiplexing to sensing.

Funding. National Natural Science Foundation of China (61890961); Natural Science Basic Research Program of Shaanxi Province (2018JM6008).

Disclosures. The authors declare no conflicts of interest.

Data availability. Data underlying the results presented in this paper are not publicly available at this time but may be obtained from the authors upon reasonable request.

References

- D. Dai, "Silicon Nanophotonic Integrated Devices for On-Chip Multiplexing and Switching," J. Lightwave Technol. 35(4), 572–587 (2017).
- T. A. Eriksson, T. Hirano, B. J. Puttnam, G. Rademacher, R. S. Luís, M. Fujiwara, R. Namiki, Y. Awaji, M. Takeoka, N. Wada, and M. Sasaki, "Wavelength division multiplexing of continuous variable quantum key distribution and 18.3 Tbit/s data channels," Commun. Phys. 2(1), 9 (2019).
- D. Dai, C. Li, S. Wang, H. Wu, Y. Shi, Z. Wu, S. Gao, T. Dai, H. Yu, and H.-K. Tsang, "10-Channel Mode (de)multiplexer with Dual Polarizations," Laser Photonics Rev. 12(1), 1700109 (2018).
- S. Pathak, P. Dumon, D. Van Thourhout, and W. Bogaerts, "Comparison of AWGs and Echelle Gratings for Wavelength Division Multiplexing on Silicon-on-Insulator," IEEE Photon. J. 6(5), 1–9 (2014).
- N. A. Idrisa and H. Tsuda, "6.4-THz-spacing, 10-channel cyclic arrayed waveguide grating for T- and O-band coarse WDM," IEICE Electron. Expr. 13(7), 1–7 (2016).
- N. A. Idris, N. Yamamoto, K. Akahane, K. Yoshizawa, Y. Tomomatsu, M. Sudo, T. Hajikano, R. Kubo, T. Uesugi, T. Kikuchi, and H. Tsuda, "A WDM/TDM Access Network Based on Broad T-Band Wavelength Resource Using Quantum Dot Semiconductor Devices," IEEE Photon. J. 8(1), 1–10 (2016).
- J. N. Kemal, P. Marin-Palomo, V. Panapakkam, P. Trocha, S. Wolf, K. Merghem, F. Lelarge, A. Ramdane, S. Randel, W. Freude, and C. Koos, "Coherent WDM transmission using quantum-dash mode-locked laser diodes as multi-wavelength source and local oscillator," Opt. Express 27(22), 31164–31175 (2019).
- S. J. Kim, S. Choi, C. Choi, Y. Lee, J. Sung, H. Yun, J. Jeong, S. E. Mun, Y. W. Lee, and B. Lee, "Broadband efficient modulation of light transmission with high contrast using reconfigurable VO2 diffraction grating," Opt. Express 26(26), 34641–34654 (2018).
- S. Sharma, V. Kumar, P. Rawat, J. Ghosh, and V. Venkataraman, "Nanowaveguide Designs in 220-nm SOI for Ultra-Broadband FWM at Telecom Wavelengths," IEEE J. Quantum Electron. 56(5), 1–8 (2020).
- K. Nakajima, J. Zhou, K. Tajima, K. Kurokawa, C. Fukai, and I. Sankawa, "Ultra Wide Band 190 Gbits WDM Transmission over a Long Length and Low Loss PCF," Optical Fiber Communication Conference Technical Digest (CD), paper PD23 (2004).
- X. Pommarede, K. Hassan, P. Billondeau, V. Hugues, P. Grosse, B. Charbonnier, and G. H. Duan, "16×100 GHz Echelle Grating-Based Wavelength Multiplexer on Silicon-on-Insulator Platform," IEEE Photonics Technol. Lett. 29(6), 493–495 (2017).
- 12. R. J. Lycett, D. F. G. Gallagher, and V. J. Brulis, "Perfect Chirped Echelle Grating Wavelength Multiplexor: Design and Optimization," IEEE Photon. J. 5(2), 2400123 (2013).
- D. Z. Feng, N. N. Feng, C. C. Kung, H. Liang, W. Qian, J. Fong, B. J. Luff, and M. Asghari, "Compact single-chip VMUX/DEMUX on the silicon-on-insulator platform," Opt. Express 19(7), 6125–6130 (2011).
- K. Li, J. Zhu, Y. Mao, N. Zhang, and X. Hou, "Design of efficient concave diffraction grating on 220 nm SOI platform for hybrid WDM–PDM (de)multiplexing," Opt. Commun. 477, 126358 (2020).
- P. Pottier and M. Packirisamy, "Design and Properties of Concave Diffraction Gratings Based on Elliptical Bragg Mirrors," J. Lightwave Technol. 31(12), 1890–1898 (2013).

- C. Sciancalepore, R. J. Lycett, J. A. Dallery, S. Pauliac, K. Hassan, J. Harduin, H. Duprez, U. Weidenmueller, D. F. G. Gallagher, S. Menezo, and B. B. Bakir, "Low-Crosstalk Fabrication-Insensitive Echelle Grating Demultiplexers on Silicon-on-Insulator," IEEE Photonics Technol. Lett. 27(5), 494

 –497 (2015).
- W.-C. Kim, Y.-S. Kim, S.-Y. Kim, Y.-C. Noh, Y.-K. Song, S.-H. Kang, J.-G. Pyo, and J.-B. Kim, "Investigation of 18-channel CWDM arrayed waveguide grating with silica-based waveguide," Opt. Eng. 55(8), 087110 (2016).
- R. Cheng, C. L. Zou, X. Guo, S. Wang, X. Han, and H. X. Tang, "Broadband on-chip single-photon spectrometer," Nat. Commun. 10(1), 4104 (2019).
- M. Yang, M. Li, and J. He, "Polarization insensitive arrayed-input spectrometer chip based on silicon-on-insulator echelle grating," Chin. Opt. Lett. 15(8), 081301 (2017).
- E. Ryckeboer, A. Gassenq, M. Muneeb, N. Hattasan, S. Pathak, L. Cerutti, J. B. Rodriguez, E. Tournie, W. Bogaerts, R. Baets, and G. Roelkens, "Silicon-on-insulator spectrometers with integrated GalnAsSb photodiodes for wide-band spectroscopy from 1510 to 2300 nm," Opt. Express 21(5), 6101–6108 (2013).
- Y. Mao, J. Zhu, K. Li, B. Du, and X. Hou, "Perfect matching of concave diffraction grating with continuously circular Bragg mirrors on SOI platform," J. Opt. Soc. Am. A 36(4), 641–646 (2019).
- J. Brouckaert, W. Bogaerts, S. Selvaraja, P. Dumon, R. Baets, and D. Van Thourhout, "Planar Concave Grating Demultiplexer With High Reflective Bragg Reflector Facets," IEEE Photonics Technol. Lett. 20(4), 309–311 (2008).
- F. Horst, W. M. J. Green, B. J. Offrein, and Y. A. Vlasov, "Silicon-on-Insulator Echelle Grating WDM Demultiplexers With Two Stigmatic Points," IEEE Photonics Technol. Lett. 21(23), 1743–1745 (2009).
- 24. G. C. Righini, F. Horst, S. K. Honkanen, W. M. J. Green, B. J. Offrein, L. Pavesi, L. Vivien, and Y. Vlasov, "Echelle grating WDM (de-)multiplexers in SOI technology, based on a design with two stigmatic points," Proc. SPIE 6996, 699660 (2008).
- P. Yeh, A. Yariv, and C.-S. Hong, "Electromagnetic propagation in periodic stratified media. I. General theory," J. Opt. Soc. Am. 67(4), 423–438 (1977).
- A. Yariv and P. Yeh, "Electromagnetic propagation in periodic stratified media. II. Birefringence, phase matching, and x-ray lasers," J. Opt. Soc. Am. 67(4), 438–448 (1977).
- B. Du, J. Zhu, Y. Mao, K. Wang, H. Chen, and X. Hou, "Effects of tilted angle of Bragg facets on the performance of successive strips based Bragg concave diffraction grating," Opt. Commun. 410, 338–344 (2018).
- L.-L. Lin, Z.-Y. Li, and K.-M. Ho, "Lattice symmetry applied in transfer-matrix methods for photonic crystals," J. Appl. Phys. 94(2), 811–821 (2003).
- 29. B. Du, J. Zhu, Y. Mao, B. Li, Y. Zhang, and X. Hou, "A design method based on photonic crystal theory for Bragg concave diffraction grating," Opt. Commun. 385, 92–96 (2017).
- W. Bogaerts, S. K. Selvaraja, P. Dumon, J. Brouckaert, K. De Vos, D. Van Thourhout, and R. Baets, "Silicon-on-Insulator Spectral Filters Fabricated With CMOS Technology," IEEE J. Select. Topics Quantum Electron. 16(1), 33–44 (2010).
- 31. P. Pottier, M. J. Strain, and M. Packirisamy, "Integrated Microspectrometer with Elliptical Bragg Mirror Enhanced Diffraction Grating on Silicon on Insulator," ACS Photonics 1(5), 430–436 (2014).
- 32. K. Ma, K. Chen, N. Zhu, L. Liu, and S. He, "High-Resolution Compact On-Chip Spectrometer Based on an Echelle Grating With Densely Packed Waveguide Array," IEEE Photon. J. 11(1), 1–7 (2019).